Pd_6CuB_3 - a new structure type of borides. Th_7Fe_3-type derivative structures in Pd(Pt)-Cu-B systems.

Leonid P. Salamakha,[a] Oksana Sologub,*[a] Berthold Stöger,[b] Peter F. Rogl,[c] Monika Waas,[a] Herwig Michor,[a] Ernst Bauer[a]

[a] Dr. L.P. Salamakha, Dr. O. Sologub, M. Waas, Prof. H. Michor, Prof. E. Bauer
Institute of Solid State Physics
TU Wien
Wiedner Hauptstraße 8-10, A-1040 Vienna, Austria
E-mail: *oksana.sologub@univie.ac.at*

[b] Dr. . B. Stöger
Institute for Chemical Technologies and Analytics
TU Wien
Getreidemarkt 9/164, A-1060 Vienna, Austria

[c] Prof. P.F. Rogl
Institute of Materials Chemistry and Research
University of Vienna
Währingerstrasse 42, A-1090 Vienna, Austria

Supporting information for this article is available on the WWW under http:\\

Abstract: A missing member of the series of Th_7Fe_3-type derivative structures, *h*-$(Pd_{0.864}Cu_{0.136})_7B_3$ (unique structure type Pd_6CuB_3, space group $P6_3cm$, a=12.9426(9) Å, c=4.8697(4) Å) was obtained from as cast alloys and alloys annealed at 600 °C - 650 °C. Further substitution of Cu by Pd led to formation of a Mn_7C_3-type structure, *o*-$(Pd_{0.93}Cu_{0.07})_7B_3$ (space group *Pnma*, a=4.8971(2) Å, b=7.5353(3) Å, c=12.9743(6) Å). Isotypic *h*-$(Pt_{0.70}Cu_{0.30})_7B_3$ was observed in the Pt-Cu-B system as a low temperature phase (T≤600 °C), whereas the B-filled Th_7Fe_3-type (HT *h*-$(Pt_{0.717}Cu_{0.283})_7B_{3+x}$, space group $P6_3mc$, a=7.4424(12) Å, c=4.8549(8) Å) proved to be stable at high temperature. The three structures are built of columns of face connected metal octahedra and columns of metal tetrahedra alternatingly fused by common faces and vertices. Boron atoms are found in trigonal prisms formed by metal atoms; additionally octahedral boron coordination was encountered in HT *h*-$(Pt_{0.717}Cu_{0.283})_7B_{3+x}$. A superconductivity was discovered for $Pt_{4.9}Cu_{2.1}B_3$ (Pd_6CuB_3-type) and $Pt_{5.04}Cu_{1.96}B_{3.3}$ (B-filled Th_7Fe_3-type) below 0.67 and 0.66 K, respectively. Despite the close value of the transition temperature the values of the upper critical field at 0 K differ as 0.37 T and 0.27 T for the two compounds.

Introduction

The Th_7Fe_3-type structure (space group $P6_3mc$, a=9.85 Å, *c*=6.15 Å, Th1 in octahedral site 6*c*, Th2 and Th3 in tetrahedral sites 6*c* and 2*b* respectively, Fe in trigonal prismatic void in 6*c*),[1] which is particularly common among the rare earth - transition metal (M) binary systems, is also adopted by transition metal carbides and borides. Atomic arrangements of the Th_7Fe_3 type carbides, so-called polytypes of the Eckstrom-Adcock phase,[2] attract continuous research interest from the materials science community because of the significance of these compounds in manufacturing of chromium steels, high-alloyed cast irons and other engineering materials.[3-6] The M_7C_3 carbide structures usually exhibit many planar defects;[7] an extensive investigation of these defects in M_7C_3 (M=Cr, Fe) crystals by electron diffraction and resulting structures were presented by Kowalski (1985).[8] Nevertheless, the hexagonal $P6_3mc$[9] and orthorhombic *Pnma*[10] unit cells (Th_7Fe_3- and Mn_7C_3-type structure, respectively) have been commonly considered for M_7C_3 transition metal carbides. Very recently, a new orthorhombic *o*-Fe_7C_3[11] phase (a=4.5202 Å, b=13.7572 Å, c=11.974 Å) isotypic with the Ca_7Au_3-type (space group *Pbca*)[12] has been derived from high-pressure single crystal X-ray diffraction data. In contrast to transition metal carbide systems, only few binary transition metal borides were found to crystallize in the Th_7Fe_3-type structure: Ru_7B_3,[9] Rh_7B_3,[13] Re_7B_3,[13] and Tc_7B_3[14]. Besides, a disordered variant of Th_7Fe_3 has been reported

recently for a metastable Ni_7B_3 compound.[15] M/M' substitution has been studied for Re_7B_3 by Kuz'ma et al. (M'=Co, Ni, Nb, Hf, Ta)[16] and for Ru_7B_3 and Rh_7B_3 by Fokwa et al. (M'= Cr, Mn, Fe, Co, Ni)[17]. Comparative studies of the structures of Rh_7B_3, Ru_7B_3 and Re_7B_3 binaries in relation to M_7C_3 carbides[18] elucidated the hexagonal symmetry for M_7B_3 and revealed the absence of either superstucture reflections or diffuse intensities thus confirming the structure of borides as suggested by Aronsson[9,13].

Considering (i) the fact that boron and carbon tend to form homologues compounds at low non-metal contents (e.g. $Cr_{23}C_6$-type, Fe_3C-type, etc.)[19] as well as (ii) the ambiguity in solving complex boride structures based on powder diffraction data, the absence of Th_7Fe_3-type derivative structures among borides was intriguing. Our recent work into Pd(Pt)-Cu-B systems[20,21] exemplified the potential of boride and carbide systems to exhibit common structural arrangements, which still have to be synthesized. Herein we report the discovery of a novel series of ternary metal borides of the Th_7Fe_3 family, among which the hexagonal *h*-$(Pd_{0.864}Cu_{0.136})_7B_3$ adopts a new structure type, the Pd_6CuB_3 type, whereas orthorhombic *o*-$(Pd_{0.93}Cu_{0.07})_7B_3$ (Mn_7C_3-type) has never been observed before among transition metal borides. The hexagonal structure discovered is apparently so far a missing member of the structural series exhibiting a volume ratio of 1 (Th_7Fe_3-type) : 2 (Mn_7C_3-type) : 3 (Pd_6CuB_3-type) : 4 (Ca_7Au_3-type). We also report in the current work on a B-filled Th_7Fe_3-type, which was observed for the first time from as cast alloys in the Pt-Cu-B system while the samples annealed at 600 °C showed isotypism with the novel Pd_6CuB_3-type. The structures of all three new borides were determined by single-crystal X-ray diffraction and confirmed from Rietveld refinements of powder X-ray diffraction data; we should note that the current study on the orthorhombic Th_7Fe_3-derivative boride is the first one performed from single crystal intensity data since the discovery of this structural arrangement from Weissenberg photographs in 1969[10]. The relationships between the new structure type and the three derivatives of Th_7Fe_3-type are discussed. We present herein as well the electrical transport properties down to 0.3 K for four compounds including the evaluation of upper critical fields of the new superconductors $Pt_{4.9}Cu_{2.1}B_3$ (Pd_6CuB_3-type) and $Pt_{5.04}Cu_{1.96}B_{3.3}$ (B-filled Th_7Fe_3-type); the results obtained have provided impetus for further investigation of physical properties of these compounds which will be reported in a forthcoming paper. Because the structural studies of transition metal carbides are challenging owing to experimental difficulties arising from the highly faulted nature of MM'_7C_3 crystals[7,8], the obtained crystallographic data on homologues boride structures are significant for further development of the important technological materials.

Results and Discussion

Crystal structure of HT *h*-$(Pt_{0.717}Cu_{0.283})_7B_{3+x}$, x=0.28. The positions of heavy atoms and B1 obtained from structure refinement in the space group $P6_3mc$ from X-ray single crystal data (Tables 1-2) are consistent with the Th_7Fe_3-type[1]. Accordingly, metal atoms in the structure of platinum copper boride (Figure 1) are distributed within the three thorium atom sites, two of which randomly accommodate Pt and Cu atoms (M2 in 6*c* and M3 in 2*b,* respectively). The Th1 octahedral site is solely occupied by platinum (Pt1 in 6*c*); about 30% of [$Pt1_6$] octahedra are centered by additional boron atoms (B2 in 2*a*). Coordination polyhedra of atoms are shown in Figure1 Supporting Information. B1 is found at the iron atom site inside a trigonal prism formed by metal atoms. The B-metal atom distances in trigonal prisms are ranging within 2.00 Å and 2.19 Å (Table 1 Supporting Information); two additional M2 atoms are located against the rectangular faces of the prism at a distance of 0.268 nm. The shortest contact of 2.00 Å between boron and Pt1 in the [$B2Pt_6$] octahedron is not unusual considering partial occupancy of the boron atom site. Atoms M2 and M3 are coordinated by 15 atoms. The coordination number of Pt1 has increased to 16 as compared to the corresponding metal atom in boride representatives of Th_7Fe_3-type, e.g. Ru in Ru_7B_3 due to two extra B2 atoms delivered by a new boron site centering the [$Pt1_6$] octahedra.

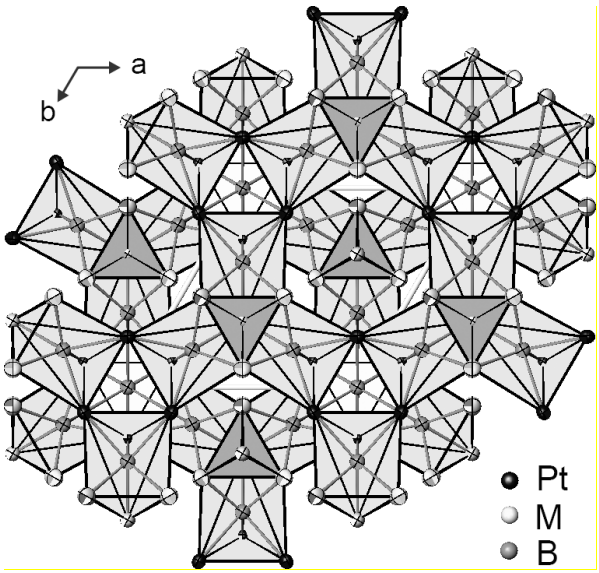

Figure 1. Crystal structure of HT *h*-$(Pt_{0.717}Cu_{0.283})_7B_{3+x}$, x=0.28 as arrangement of B filled trigonal prisms (grey; in online version - orange), B filled octahedra (light grey; in online version - yellow) and empty tetrahedra (dark grey; in online version - green).

Table 1. Crystallographic data[a] for HT *h*-$(Pt_{0.717}Cu_{0.283})_7B_{3+x}$, x=0.28 (B-filled Th_7Fe_3-type), *h*-$(Pd_{0.864}Cu_{0.136})_7B_3$ (Pd_6CuB_3-type) and *o*-$(Pd_{0.93}Cu_{0.07})_7B_3$ (Mn_7C_3-type).

structure type	B-filled Th_7Fe_3	Pd_6CuB_3	Mn_7C_3
composition	$Pt_{5.02}Cu_{1.98}B_{3.28}$	$Pd_{6.047}Cu_{0.953}B_3$	$Pd_{6.504}Cu_{0.496}B_3$
space group	$P6_3mc$, no. 186	$P6_3cm$, no. 185	*Pnma*, no.62
lattice parameters			
a [Å]	7.4424(12)	12.9426(9)	4.8971(2)
b [Å]			7.5353(3)
c [Å]	4.8549(8)	4.8697(4)	12.9743(6)
V [Å^3]	232.88(7)	706.44(9)	478.77(4)
ρ_{calc} [g cm^{-3}]	16.264	10.385	10.489
Z	2	6	4
radiation, λ [Å]		MoKα, 0.71073	
2θmax [°]	61.40	60.06	65.28
N(hkl)measured	5202	12649	1495
N(hkl)unique	281	738	1369
N(hkl)observed (F_{hkl}>4σ(F))	251	551	1173
refined parameters	26	47	50
goodness of fit	1.041	1.036	1.076
$R_F^2 = \Sigma\|F_o^2-F_c^2\|/\Sigma F_o^2$	0.0285	0.0252	0.0247
extinction coefficient	0.0004(4)	0.00004(5)	0.00047(8)
residual electron density [e Å^{-3}]	+4.31; -2.54	+1.593; -1.507	+1.237; -2.316

[a] atom coordinates are standardized using the program Structure Tidy[22]

Table 2. Atomic coordinates and equivalent isotropic displacement parameters (in [Å^2]) for HT *h*-$(Pt_{0.717}Cu_{0.283})_7B_{3+x}$, x=0.28, *h*-$(Pd_{0.864}Cu_{0.136})_7B_3$ and *o*-$(Pd_{0.93}Cu_{0.07})_7B_3$.

Atom	Site	x	y	z	Occupancy	U_{eq}[a,b]
HT *h*-$(Pt_{0.717}Cu_{0.283})_7B_{3+x}$, x=0.28						
Pt1	6*c*	0.12645(6)	0.87355	0.237(9)	1.00	0.0126(3)
M2	6*c*	0.5477(1)	0.4523(1)	0.069(9)	0.446(3)Pt2+0.554(3)Cu2	0.0164(4)
M3	2*b*	⅓	⅔	0.048(9)	0.681(4)Pt3+0.319(4)Cu3	0.0165(5)
B1	6*c*	0.813(2)	0.187(2)	0.342(11)	1.00	0.014(5)
B2	2*a*	0	0	0.000[c]	0.28(7)	0.014(5)
***h*-$(Pd_{0.864}Cu_{0.136})_7B_3$**						
Pd1	12*d*	0.20828(8)	0.54320(8)	0.3674(2)	1.00	0.0071(2)
M2	12*d*	0.2075(1)	0.3315(2)	0.1765(3)	0.627(4)Pd2+0.373(4)Cu2	0.0095(3)
Pd3	6*c*	0.3352(2)	0	0.1901(5)	1.00	0.0088(2)
Pd4	6*c*	0.1233(1)	0	0.0000[c]	1.00	0.0073(3)
M5	6*c*	0.5498(1)	0	0.2186(4)	0.793(4)Pd5+0.207(4)Cu5	0.0088(4)
B1	12*d*	0.324(1)	0.474(1)	0.470(3)	1.00	0.011(1)
B2	6*c*	0.193(2)	0	0.399(4)	1.00	0.011(1)
o-$(Pd_{0.93}Cu_{0.07})_7B_3$						
Pd1	8*d*	0.06598(6)	0.56369(4)	0.31094(3)	1.00	0.0070(1)
M2	8*d*	0.24897(7)	0.06486(5)	0.01827(3)	0.786(3)Pd2+0.214(3)Cu2	0.0090(1)
Pd3	4*c*	0.23498(9)	¼	0.41479(4)	1.00	0.0067(1)
Pd4	4*c*	0.42506(9)	¼	0.62647(3)	1.00	0.0067(1)
M5	4*c*	0.2081(1)	¼	0.20098(4)	0.932(3)Pd5+0.068(3)Cu5	0.0073(1)
B1	8*d*	0.461(1)	0.0317(7)	0.3510(4)	1.00	0.011(1)
B2	4*c*	0.033(1)	¼	0.5609(6)	1.00	0.014(1)

[a] U_{eq} is defined as one-third of the trace of the orthogonalized U_{ij} tensor; [b] anisotropic displacement parameters are listed in Table 2 Supporting Information; [c] fixed parameter

Table 1 Supporting Information. Selected interatomic distances [Å]

HT *h*-$(Pt_{0.717}Cu_{0.283})_7B_{3+x}$, x=0.28[a]

Pt1– B2 2.00(3)	M2- 2B1 2.19(5)	M3– 3B1 2.13(4)	B1 - Pt1 2.07(3)	B2 - 3 Pt1 2.00(3)
- B2 2.07(3)	- 2M2 2.655(3)	-3M2 2.766(3)	- M3 2.13(4)	- 3 Pt1 2.07(3)
- B1 2.07(3)	- 2B1 2.68(3)	-3M2 2.777(2)	- 2Pt1 2.19(3)	
- 2B1 2.19(3)	- 2M2 2.722(1)	-3Pt1 2.82(3)	- 2M2 2.19(5)	
- M3 2.82(3)	- M3 2.766(3)	-3M2 2.97(6)	- 2M2 2.68(3)	
- 2Pt1 2.823(2)	- M3 2.777(2)			
- 2M2 2.83(4)	- 2Pt1 2.83(4)			
- 2M2 2.84(2)	- 2Pt1 2.84(2)			
- 4Pt1 2.92(6)	- M3 2.97(6)			

***h*-$(Pd_{0.864}Cu_{0.136})_7B_3$**[b]

Pd1– B1 2.11(1)	M2- B2 2.17(2)	Pd3– B2 2.10(2)	Pd4– B2 2.14(2)	M5- 2B1 2.19(2)
- B1 2.16(1)	- B1 2.22(1)	-2B1 2.15(1)	- 2B2 2.25(2)	- 2M2 2.729(2)
- B1 2.26(2)	- B1 2.51(2)	-2M2 2.711(4)	- 2Pd4 2.765(2)	- Pd3 2.763(3)
-2Pd1 2.786(2)	- B2 2.60(2)	- M5 2.736(3)	- M2 2.824(2)	- 2M5 2.755(3)
- M2 2.824(2)	- 2M2 2.664(2)	- M5 2.780(3)	- M2 2.824(2)	- Pd3 2.780(3)
- Pd3 2.829(3)	- Pd3 2.711(4)	-2Pd1 2.829(3)	- 2M2 2.827(2)	- 2Pd1 2.834(1)
- M5 2.834(1)	- M5 2.729(2)	-2M2 2.875(2)	- Pd3 2.895(3)	- 2Pd1 2.900(2)
- M2 2.889(2)	- M2 2.780(3)	- Pd4 2.895(3)	- 4Pd4 2.911(1)	- Pd3 2.973(3)
- M5 2.900(2)	- Pd4 2.824(2)	- M5 2.973(3)		
-2Pd1 2.901(1)	- Pd1 2.824(2)	- 2M2 2.985(3)	B2 - Pd3 2.10(2)	B1 - Pd1 2.11(1)
-2Pd1 2.935(2)	- Pd4 2.827(2)		- Pd4 2.14(2)	- Pd3 2.15(1)
	- Pd3 2.875(2)		- 2M2 2.17(2)	- Pd1 2.16(1)
	- Pd1 2.889(2)		- 2Pd4 2.25(2)	- M5 2.19(2)
	- Pd3 2.985(3)		- 2M2 2.60(2)	- M2 2.22(1)
				- Pd1 2.26(2)
				- M2 2.51(2)

***o*-$(Pd_{0.93}Cu_{0.07})_7B_3$**[c]

Pd1– B1 2.127(5)	M2- B1 2.221(5)	Pd3– B2 2.139(8)	Pd4– B2 2.101(7)	M5- 2B1 2.151(5)
- B2 2.229(6)	- B2 2.221(6)	-2B1 2.148(5)	- 2B1 2.215(5)	- 2M2 2.729(2)
- B1 2.280(5)	- B1 2.509(5)	-2M2 2.7272(5)	- 2Pd1 2.7751(5)	- 2M5 2.7592(7)
- Pd4 2.7751(5)	- B2 2.660(3)	- M5 2.7610(7)	- 2Pd2 2.8265(5)	- Pd3 2.7610(7)
- Pd1 2.8078(4)	- M2 2.6695(5)	- M5 2.7772(7)	- 2Pd2 2.8855(5)	- Pd3 2.7772(7)
- Pd2 2.8385(6)	- M2 2.6880(5)	-2Pd1 2.8439(4)	- Pd3 2.8999(7)	- 2Pd1 2.8472(5)
- Pd3 2.8439(4)	- Pd3 2.7272(5)	-2M2 2.8923(5)	- 2Pd1 2.9005(5)	- 2Pd1 2.9468(4)
- Pd5 2.8472(5)	- M5 2.7579(6)	- Pd4 2.8999(7)	- 2Pd1 2.9737(5)	- Pd3 2.9857(7)
- Pd2 2.8738(5)	- M2 2.7902(5)	- M5 2.9857(7)		
- Pd4 2.9005(5)	- Pd4 2.8265(5)	- 2M2 3.0060(6)	B2 - Pd4 2.101(7)	B1 - Pd1 2.127(5)
-2Pd1 2.9148(5)	- Pd1 2.8385(6)		- Pd3 2.139(8)	- Pd3 2.148(5)
- Pd5 2.9468(4)	- Pd1 2.8738(5)		- 2M2 2.221(6)	- M5 2.151(5)
- Pd4 2.9737(5)	- Pd4 2.8855(5)		- 2Pd1 2.229(6)	- Pd4 2.215(5)
	- Pd3 2.8923(5)		- 2M2 2.660(3)	- M2 2.221(5)
	- Pd3 3.0060(6)			- Pd1 2.280(5)
				- M2 2.509(5)

[a]M2=0.446(3) Pt2+0.554(3)Cu2, M3=0.681(4)Pt3+0.319(4)Cu3
[b]M2=0.627(4) Pd2+0.373(4)Cu2, M5=0.793(4)Pd5+0.207(4)Cu5
[c]M2=0.786(3)Pd2+0.214(3)Cu2, M5=0.932(3)Pd5+0.068(3)Cu5

Crystal structure of *h*-$(Pd_{0.864}Cu_{0.136})_7B_3$ - a new Pd_6CuB_3-type. The compound represents a unique type of the Th_7Fe_3 derivative structures where palladium atoms occupy two octahedral sites (Pd1 in 12*d* and Pd4 in 6*c*) and one tetrahedral site (Pd3 in 6*c*) while the remaining two tetrahedral sites are randomly populated by Pd and Cu (M2 in 12*d* and M5 in 6*c*) (Tables 1-2, Figure 2). Trigonal prisms formed by metal atoms with one (and two) additional M2 atoms against their rectangular faces accommodate B1 and B2 respectively

(Table 1 Supporting Information, Figure 1k,l Supporting Information). The [$Pd1_6$] and [$Pd4_6$] octahedra are not occupied by boron in the current crystal. Both Pd1 and Pd4 are coordinated by 11 metal atoms and 3 borons. Similarly to M3 in HT *h*-$(Pt_{0.717}Cu_{0.283})_7B_{3+x}$ of B-filled Th_7Fe_3-type, the Pd3 have 15 neighbors; M2 and M5 are bounded to 15 and 13 atoms respectively.

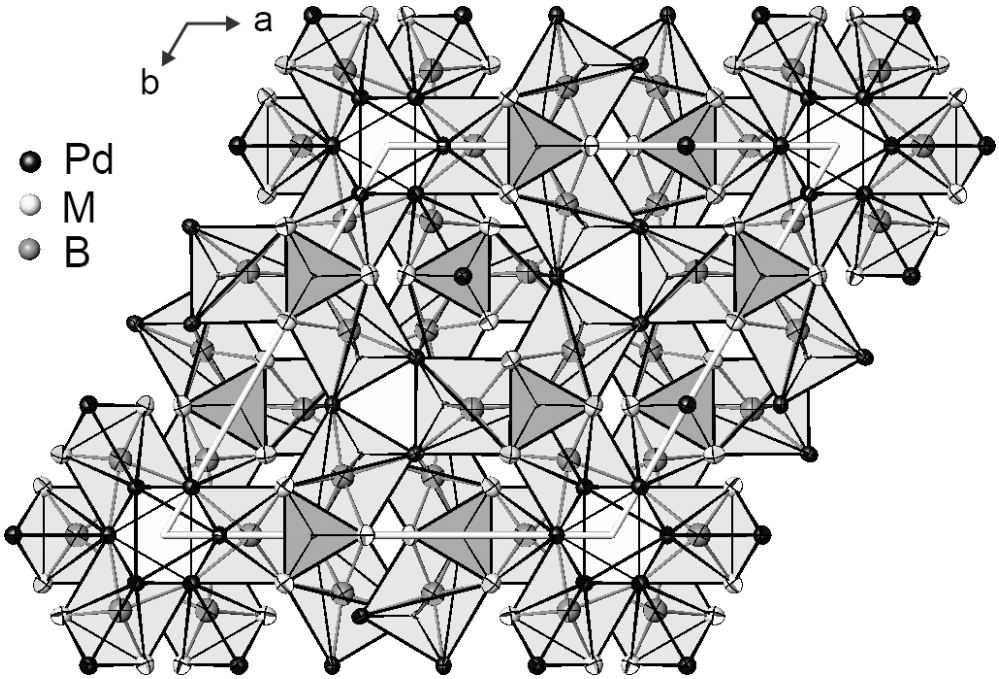

Figure 2. Crystal structure of *h*-$(Pd_{0.864}Cu_{0.136})_7B_3$ as arrangement of B-filled trigonal prisms (grey; in online version - orange), empty octahedra (light grey; in online version - yellow) and empty tetrahedra (dark grey; in online version - green).

Table 2 Supporting Information. Anisotropic displacement parameters (in [Å^2]) for HT *h*-$(Pt_{0.717}Cu_{0.283})_7B_{3+x}$, x=0.28, *h*-$(Pd_{0.864}Cu_{0.136})_7B_3$ and *o*-$(Pd_{0.93}Cu_{0.07})_7B_3$.

Atom	Site	U_{11}	U_{22}	U_{33}	U_{23}	U_{13}	U_{12}
HT *h*-$(Pt_{0.717}Cu_{0.283})_7B_{3+x}$, x=0.28							
Pt1	6*c*	0.0095(4)	0.0095(4)	0.0204(5)	-0.0008(2)	0.0008(2)	0.0059(3)
M2	6*c*	0.0132(6)	0.0132(6)	0.0216(9)	-0.0042(3)	0.0042(3)	0.0056(6)
M3	2*b*	0.00942(6)	0.00942(6)	0.0307(12)	0	0	0.0047(3)
***h*-$(Pd_{0.864}Cu_{0.136})_7B_3$**							
Pd1	12*d*	0.0066(4)	0.0068(4)	0.0071(4)	0	-0.0002(5)	0.0026(4)
M2	12*d*	0.0084(7)	0.0107(6)	0.0094(6)	0.0000(3)	0.0006(5)	0.0045(6)
Pd3	6*c*	0.0080(5)	0.0082(9)	0.0102(4)	0	0.0005(3)	0.0041(5)
Pd4	6*c*	0.0068(5)	0.0080(7)	0.0075(7)	0	-0.0008(6)	0.0040(3)
M5	6*c*	0.0090(6)	0.0096(9)	0.0079(8)	0	0.0017(5)	0.0048(5)
***o*-$(Pd_{0.93}Cu_{0.07})_7B_3$**							
Pd1	8*d*	0.0076(2)	0.0070(2)	0.0063(2)	0.0009(1)	-0.0004(1)	0.0006(1)
M2	8*d*	0.0096(2)	0.0088(2)	0.0085(2)	-0.0010(1)	0.0002(1)	0.0001(1)
Pd3	4*c*	0.0075(2)	0.0069(2)	0.0058(2)	0	0.0007(2)	0
Pd4	4*c*	0.0082(2)	0.0069(2)	0.0051(2)	0	-0.0002(2)	0
M5	4*c*	0.0057(2)	0.0104(2)	0.0057(2)	0	0.0006(2)	0

Crystal structure of *o*-$(Pd_{0.93}Cu_{0.07})_7B_3$. Figure 3 shows the crystal structure of a new boride of Mn_7C_3-type[10] (Tables 1-2). As viewed along the shortest axis, the structure is composed of two columns of empty [$Pd1_4Pd4_2$] octahedra and four columns of edge- and face-connected empty [$M2_2M5Pd3$] tetrahedra (Figure 3). Coordination polyhedra of atoms and interatomic distances are given in Figure 1, Supporting Information and Table 1, Supporting Information. Alike boron atoms in the *h*-$(Pd_{0.864}Cu_{0.136})_7B_3$ structure, B1 and B2 are found in trigonal prisms formed by metal atoms. Coordination numbers of Pd1 and Pd4 and shapes of their coordination polyhedra correspond to that of Pd1 and Pd4 in the *h*-$(Pd_{0.864}Cu_{0.136})_7B_3$ structure as well as resembles the coordination polyhedron of Pt1 in the HT *h*-$(Pt_{0.717}Cu_{0.283})_7B_{3+x}$ structure, if not taking into account the surplus boron atoms delivered by populated centers of octahedra of the latter one. Analogously to Pd3 in the *h*-$(Pd_{0.864}Cu_{0.136})_7B_3$ structure of Pd_6CuB_3-type, the 15-vertices polyhedron of [$Pd3B_3M_9Pd_3$] in *o*-$(Pd_{0.93}Cu_{0.07})_7B_3$ is distorted and comprises the displacement of the B2 atom as compared to M3 in HT *h*-$(Pt_{0.717}Cu_{0.283})_7B_{3+x}$. The shape of the coordination sphere of M5 ([$M5B_2M_4Pd_7$] is analogous to that of M5 in the *h*-$(Pd_{0.864}Cu_{0.136})_7B_3$ structure.

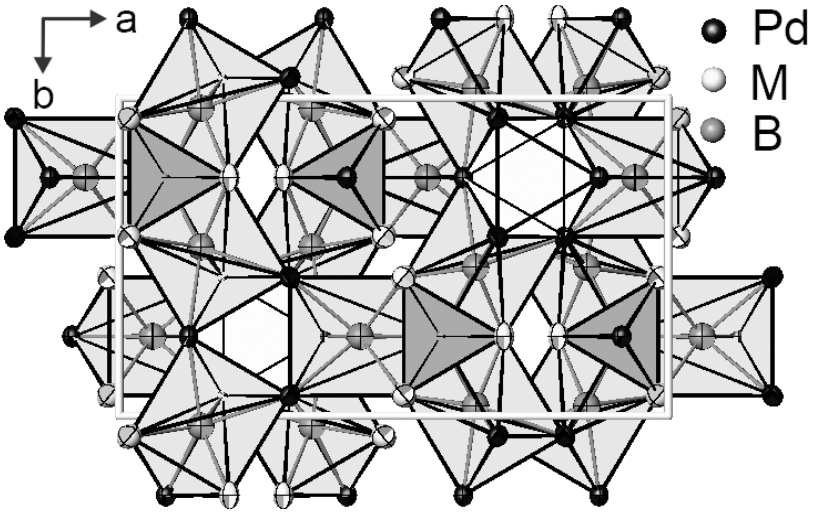

Figure 3. Crystal structure of *o*-$(Pd_{0.93}Cu_{0.07})_7B_3$ as arrangement of B-filled trigonal prisms (grey; in online version - orange), empty octahedra (light grey; in online version - yellow) and empty tetrahedra (dark grey; in online version - green).

A closer examination of coordination spheres of M2 in HT *h*-$(Pt_{0.717}Cu_{0.283})_7B_{3+x}$, *h*-$(Pd_{0.864}Cu_{0.136})_7B_3$ and *o*-$(Pd_{0.93}Cu_{0.07})_7B_3$ shows that, despite of their identical coordination numbers (CN=15), the arrangements of surrounding atoms are different. Whilst in the B-filled Th_7Fe_3-type structure, the four boron atoms coordinating the M2 site exhibit a planar orientation (Figure 4a), in the two remaining structures the boron atoms are arranged

tetrahedrally with respect to the central ones and realize, together with neighboring atoms, different geometries of the [M2Pd1$_2$Pd4$_2$M2$_3$M5$_1$Pd3$_3$B1$_2$B2$_2$] polyhedra in the *h*-(Pd$_{0.864}$Cu$_{0.136}$)$_7$B$_3$ and *o*-(Pd$_{0.93}$Cu$_{0.07}$)$_7$B$_3$ structures (Figures 4b, c, respectively).

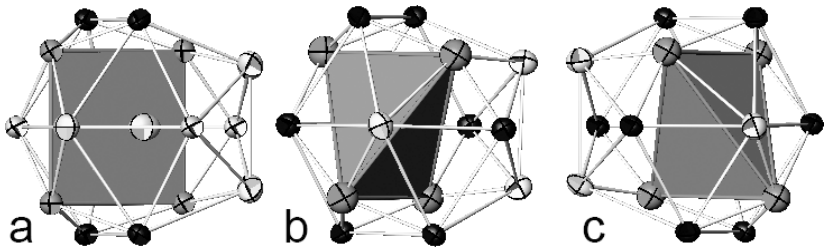

Figure 4. M2 coordination polyhedra in HT *h*-(Pt$_{0.717}$Cu$_{0.283}$)$_7$B$_{3+x}$ (a), *h*-(Pd$_{0.864}$Cu$_{0.136}$)$_7$B$_3$ (b) and *o*-(Pd$_{0.93}$Cu$_{0.07}$)$_7$B$_3$ (c) emphasizing the disposition of boron atoms in the polyhedral units. Atoms codes correspond to those given in Figures 1-3.

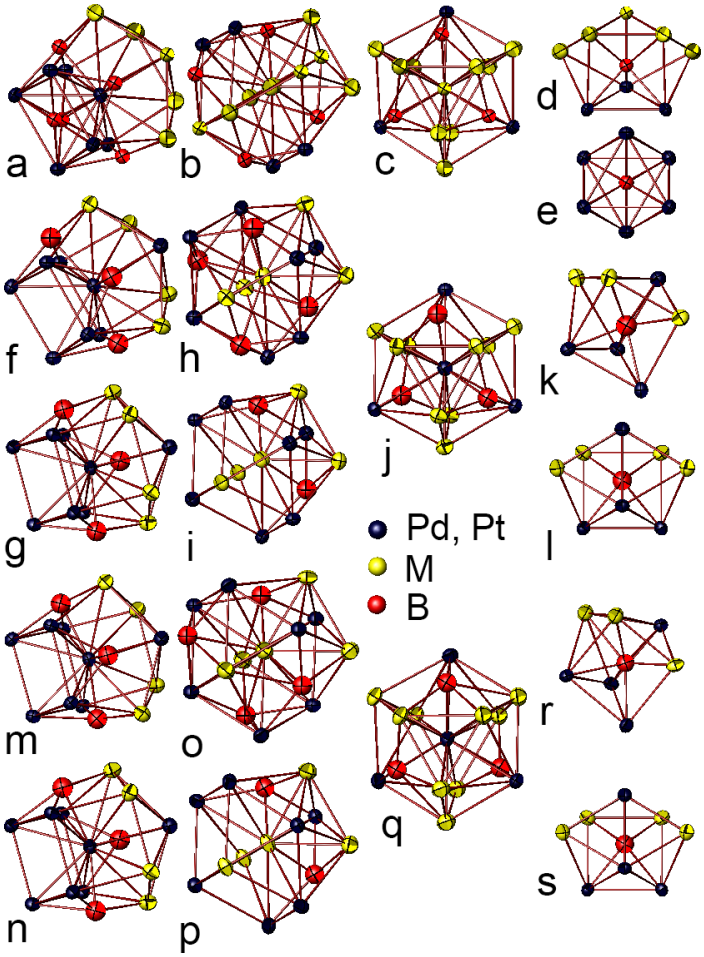

Figure 1 Supporting Information. Coordination polyhedra of atoms in the structures HT *h*-(Pt$_{0.717}$Cu$_{0.283}$)$_7$B$_{3+x}$ (a-Pt1, b-M2, c-M3, d-B1, e-B2), *h*-(Pd$_{0.864}$Cu$_{0.136}$)$_7$B$_3$ (f-Pd1, h-M2, j-Pd3, g-Pd4, i-M5, k-B1, l-B2) and *o*-(Pd$_{0.93}$Cu$_{0.07}$)$_7$B$_3$ (m-Pd1, o-M2, q-Pd3, n-Pd4, p-M5, r-B1, s-B2).

Structure relationships. All three new boride structures are closely related with the Th_7Fe_3-type[1]. According to common description,[7,23] the Th_7Fe_3 structure is composed of infinite columns of face-connected empty [$Th1_6$] octahedra and columns of empty [$Th2_3Th3_1$] tetrahedra both running infinitely along the short axis (Figure 5a-d). Tetrahedra condense alternatingly via common vertices and faces. Iron atoms are located between the columns in trigonal prisms formed by adjacent "free" faces of octahedra and tetrahedra. Every second tetrahedron in the column participates in the formation of the trigonal prisms (Figure 5d) and only half of the "free" faces of octahedra can form the bases of trigonal prisms (Figure 5c). Consequently, all prisms are sloping in one direction with respect to the short axis. Triads of [$FeTh1_3Th2_2Th3_1$] trigonal prisms, associated with successive octahedra along a column differ by 60º in orientation (Figure 5a). The trigonal prisms share edges and vertices to form a three-dimensional framework. In the parent representative of the Th_7Fe_3-type boride family, Ru_7B_3,[9] Ru substitutes for Th whereas B takes the atom site of Fe.

The HT *h*-$(Pt_{0.717}Cu_{0.283})_7B_{3+x}$ structure (B-filled variant of the Th_7Fe_3-type) and *o*-$(Pd_{0.93}Cu_{0.07})_7B_3$ (Mn_7C_3-type) differ in the relative positioning of the columns of octahedra one of which is displaced and rotated by 60° around the short axis (slab B, Figure 6b) with respect to the other (slab A, Figure 6b) in the *o*-$(Pd_{0.93}Cu_{0.07})_7B_3$ structure, while in the structure of HT *h*-$(Pt_{0.717}Cu_{0.283})_7B_{3+y}$ the columns of octahedra are identical and located at the same height along *z* (slab A, Figure 6a). Besides the Th_7Fe_3- and Mn_7C_3-type structures, a hexagonal unit cell exhibiting identical columns of octahedra but manifesting the doubled *a* and *b* lattice parameters (suggested space groups $P6_3mc$ or $P31c$, a=1.387 nm, c=0.463 nm) was hitherto also suggested[24] to describe the M_7C_3-carbides, however this structure proposal was superseded by further studies.[10,25,26]

h-$(Pd_{0.864}Cu_{0.136})_7B_3$ (Pd_6CuB_3-type) reported in the current study, exhibits a new structural arrangement which maintains the stoichiometry and structural units of the Th_7Fe_3-type structure. The unit cell of the new structure is composed of a total of three columns of face-connected metal octahedra running infinitely along the short axis, two of which are formed by Pd1 (12*d*) and one is built by Pd4 (6*c*). Thus, whilst in the *o*-$(Pd_{0.93}Cu_{0.07})_7B_3$ unit cell every second column of the existing two is moved around and along the shorter axis, *h*-$(Pd_{0.864}Cu_{0.136})_7B_3$ exhibited the arrangement of two displaced columns (slab B-B formed by Pd1) *vs* one unmoved (slab A formed by Pd4) (Figure 6c).

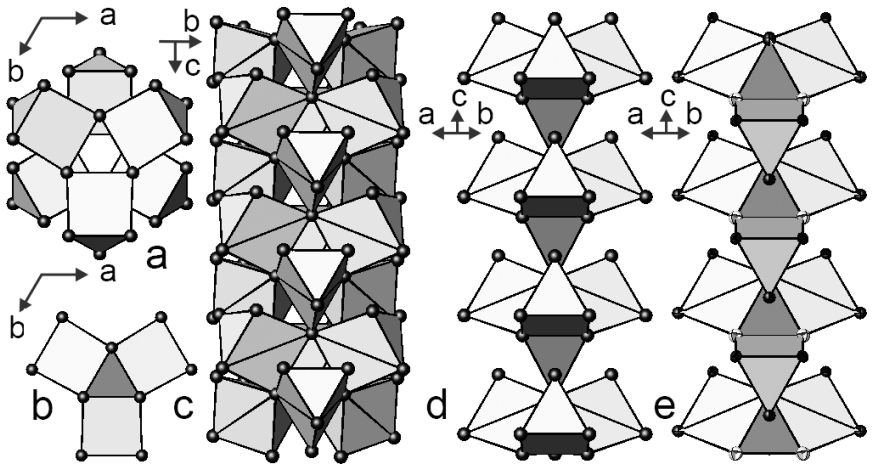

Figure 5. Boron filled trigonal metal prisms (grey; in online version - yellow) and their clustering around the columns of empty metal octahedra (left open) (a, c) and tetrahedra (dark grey; in online version - brown) (b, d) in the structure of Th_7Fe_3 extending infinitively along the short axis. Arrangements of B1 and B2 filled trigonal metal prisms (light grey and grey respectively; in online version - yellow and pink respectively) around a column of empty tetrahedra (brown) in the *h*-$(Pd_{0.864}Cu_{0.136})_7B_3$ (Pd_6CuB_3-type) structure (e). Atoms codes correspond to those given in Figures 1-3.

In the structure of HT *h*-$(Pt_{0.717}Cu_{0.283})_7B_{3+x}$ (B-filled Th_7Fe_3-type) every subsequent tetrahedron in the column offers its three "free" faces to form the bases of boron filled trigonal prisms (Figure 5d), while in the remaining structures described herein, every tetrahedron in the column participates in the formation of boron filled trigonal prisms (Figure 5e) alternatingly contributing either one or two faces. Thus the trigonal prisms attached to the tetrahedral columns are alternatively sloping up and down in the *o*-$(Pd_{0.93}Cu_{0.07})_7B_3$ (Mn_7C_3-type) and *h*-$(Pd_{0.864}Cu_{0.136})_7B_3$ (Pd_6CuB_3-type) structures.

The empty octahedron in the *o*-$(Pd_{0.93}Cu_{0.07})_7B_3$ structure (Mn_7C_3-type) is built of two kinds of Pd atoms and the resulting octahedral columns are surrounded by both B1- and B2-filled trigonal prisms. The composition and local environment of octahedra in the *h*-$(Pd_{0.864}Cu_{0.136})_7B_3$ structure (Pd_6CuB_3-type) are different from *o*-$(Pd_{0.93}Cu_{0.07})_7B_3$. The columns are composed of either $[Pd1_6]$ or $[Pd4_6]$ octahedra; each of them is surrounded by a different kind of borons. Thus the trigonal prisms around B1 and B2 in the *o*-$(Pd_{0.93}Cu_{0.07})_7B_3$ structure form a complex three-dimensional framework being connected through common edges and vertices (Figure 7b), whereas in the *h*-$(Pd_{0.864}Cu_{0.136})_7B_3$ structure the B1-filled trigonal prisms share edges and single corners to form a three-dimensional framework which envelops the columns of $[Pd4_6]$ octahedra and associated triades of $[B2Pd4_3M2_2Pd3_1]$ trigonal prisms (Figure 7a).

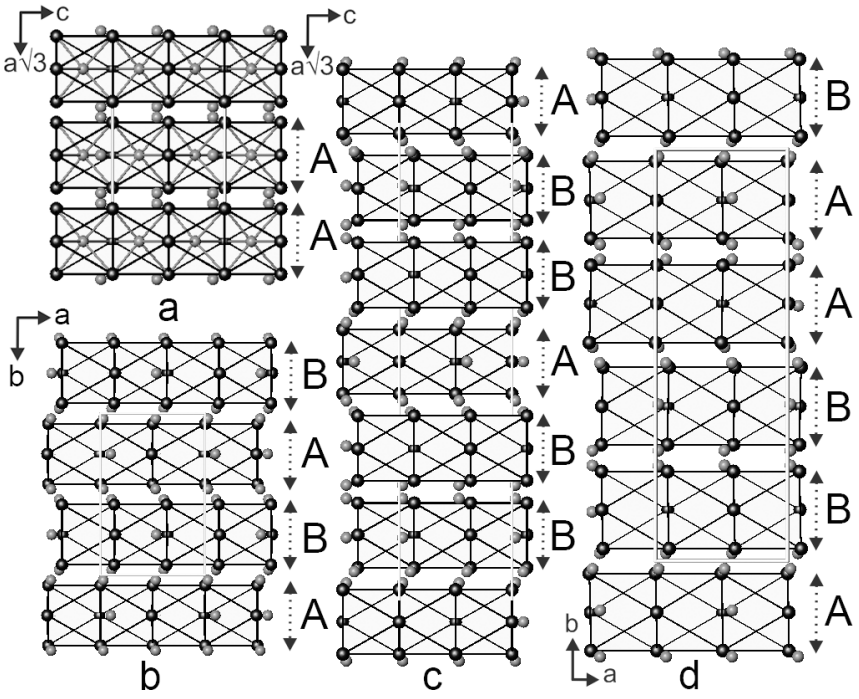

Figure 6. Arrangement of octahedra and adjacent atoms in HT *h*-$(Pt_{0.717}Cu_{0.283})_7B_{3+x}$ (a), *h*-$(Pd_{0.864}Cu_{0.136})_7B_3$ (b), *o*-$(Pd_{0.93}Cu_{0.07})_7B_3$ (c) and Ca_7Au_3 (d) structures, respectively. For better comparison, hexagonal structures are presented in orthohexagonal settings. Metal atoms which do not form octahedra are omitted. Atoms codes correspond to those given in Figure 1-3. For Ca_7Au_3 (d) - Ca is dark grey and Au is grey (in online version dark blue and red respectively).

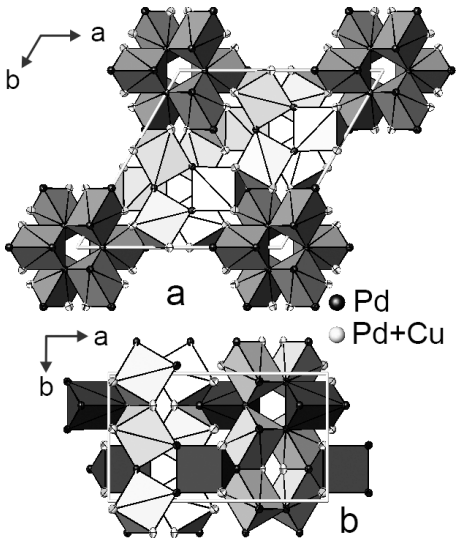

Figure 7. The frameworks of boron filled trigonal prisms (B1 - grey, B2 - dark grey; in online version yellow and pink respectively) in the structures *h*-$(Pd_{0.864}Cu_{0.136})_7B_3$ (Pd_6CuB_3-type, a) and *o*-$(Pd_{0.93}Cu_{0.07})_7B_3$ (Mn_7C_3-type, b).

All structures reported here, (HT *h*-$(Pt_{0.717}Cu_{0.283})_7B_{3+x}$ (B-filled Th_7Fe_3-type), *o*-$(Pd_{0.93}Cu_{0.07})_7B_3$ (Mn_7C_3-type), *h*-$(Pd_{0.864}Cu_{0.136})_7B_3$ (Pd_6CuB_3-type) as well as the Ca_7Au_3-type[12] structure which exhibits two A fragments *vs* two B (Figure 6d), maintain the octahedra-to-tetrahedra ratio equal to 2 and their unit cell volumes relate as 1:2:3:4, respectively, considering the existence of Ca_7Au_3-type related platinum copper boride described herein below exhibiting the lattice parameters a=4.9248 Å, b=14.563 Å, c=12.920 Å.

Formation of compounds and site preferences. The investigations of compounds with the Th_7Fe_3-type derivative structures have been focused hitherto on chromium iron carbides alloyed with additional transition metals due to dramatic influence of the eutectic MM'_7C_3 carbides on the microstructure and mechanical properties of high-chromium white cast irons.[27] According to structural studies, the orthorhombic M_7C_3 phase of Mn_7C_3-type was found for synthesis temperatures above 1200 °C. At lower temperatures the diffraction patterns indicated a hexagonal structure (space group $P6_3mc$, Th_7Fe_3-type).[28] A complete solid solution has been reported between Cr_7C_3 and Mn_7C_3[29] as well as between Cr_7C_3 and Fe_7C_3;[30] solubility of Ni and W in Cr_7C_3 was found to be smaller: $Cr_{7-x}Ni_xC_3$, x=0-0.5[29] and $Cr_{7-x}W_xC_3$, x=0.4[31]. Despite of high industrial interest, there is a lack of reliable data on solubility and preferential positions for atoms of alloying elements in the multicomponent $(M,M')_7C_3$ carbide systems (M,M'=V,Cr,Mn,Fe,Co,W).[27,32] In the Fe–Cr–V-C type alloys, vanadium substitutes either for Fe or Cr depending on the Fe/Cr ratio.[33] Recent investigations on the Co-Cr-C sub-system showed that cobalt stabilizes the orthorhombic Mn_7C_3-type structure preferring to occupy the M2 and M5 sites in the orthorhombic cell,[34] however the theoretical studies based on ab initio cohesive energies and lattice inversion method suggested the hexagonal $P6_3/mc$ structure as the most stable.[35] A comparison between the obtained energies furthermore showed that at low content, Co atoms prefer to occupy the chromium sites at the vertices of tetrahedra (2*b*). After increasing the amount of Co ($Cr_{7-x}Co_xC_3$, x≥1), the additional cobalt atoms substitute chromium in tetrahedral 6*c* and octahedral 6*c* sites; moreover, the calculations indicated that despite the energy needed for cobalt atoms to occupy octahedral sites is lower, the structure with this atom site substitution pattern (Co atoms in tetrahedral 2*b* and octahedral 6*c*) become unstable if x>1.35. Thereby at higher Co content, the octahedral site is unaffected, whereas two tetrahedral sites accommodate the Cr/Co mixtures.[35]

In the Pd-Cu-B system, both high Pd content *h*-$(Pd_{0.864}Cu_{0.136})_7B_3$ and *o*-$(Pd_{0.93}Cu_{0.07})_7B_3$ phases form directly from the melt and follow the substitution pattern reported for $Co_{6.60}Cr_{0.51}C_{2.89}$[34] where the only atom sites forming the adjacent faces of tetrahedra in the columns are prone to M/M' mixing. As inherited from X-ray powder diffraction studies and EDX, the Th_7Fe_3-type derivative palladium copper borides span over a rather wide concentration range within $Pd_{58.5}Cu_{11.5}B_{30}$ to $Pd_{68.5}Cu_{1.5}B_{30}$ at 650 °C. A hexagonal structure with a tripled unit cell of Pd_6CuB_3-type exists from $Pd_{58.5}Cu_{11.5}B_{30}$ to $Pd_{63.5}Cu_{6.5}B_{30}$ (a=12.9412(1)-12.9640(2) Å, c=4.8697(1)-4.8830(1) Å, V=706.29(1)-710.72(2) $Å^3$); increase of Pd amount stabilizes the orthorhombic Mn_7C_3-type structure ($Pd_{65}Cu_5B_{30}$ - $Pd_{68.5}Cu_{1.5}B_{30}$, a=4.8884(2)-4.9116(1) Å, b=7.5272(2)-7.5585(1) Å, c=12.9697(2)-12.9733(1) Å, V=477.23(2)-481.625(2) $Å^3$ (Figure 2 Supporting Information). As delivered by single crystal and powder X-ray diffraction data refinements, the Wyckoff sites concerned with Pd/Cu substitution in the Cu-rich side of the Th_7Fe_3-type derivative structure series are tetrahedral 12*d* and 6*c* of the tripled hexagonal unit cell yielding 55.3% Pd2+44.7% Cu2 and 73.7% Pd5+26.3% Cu5 levels of occupancy, respectively (Rietveld refinement of X-ray powder diffraction data). The Pd-richest terminus amounts appr. 1.5 at.% Cu and exhibits the only one tetrahedral site affected by Pd/Cu substitution (92.1% Pd2+7.9% Cu2 in 8*d* of orthorhombic Mn_7C_3-type unit cell) (Rietveld refinement of X-ray powder diffraction data). Although the structures of the Pd-poor and Pd-rich phases are closely related, there is no continuous remodeling of the structures upon variation in Pd content in consistency with the fact that no direct crystallographic group-subgroup relation exists. The critical amount of Cu for destabilization of large hexagonal structure and formation of the orthorhombic structure is within 6.5 and 5 at.% according to X-ray diffraction data and EDX analysis of two-phase alloys (Figure 3 Supporting Information).

According to EDX measured Pt/Cu ratios and X-ray data analysis, the Th_7Fe_3-type derivative structures in Pt-Cu-B as cast alloys were found to cover the range $Pt_{0.72-y}Cu_{0.28+y})_7B_{3+x}$ (y≅0-0.16, x≅0-0.3). The Pt-rich end (HT *h*-$(Pt_{0.72-y}Cu_{0.28+y})_7B_{3+x}$, y≅0-0.07) forms a hexagonal structure of B-filled Th_7Fe_3-type which on annealing at 600 °C decomposes to the low temperature form of Pd_6CuB_3-type (Figure 4 Supporting Information, Table 3 Supporting Information). Strong irregularities in variations of lattice parameters obtained from Rietveld refinement of X-ray powder data for HT *h*-$(Pt_{0.72-y}Cu_{0.28+y})_7B_{3+x}$ within Pt-rich and Cu-rich boundaries depending on boron content with respect to EDX Pt/Cu ratios support our results obtained from single crystal X-ray diffraction data on surplus boron

amount in the structure as a consequence of incorporation of boron atoms into the octahedral voids of the Th_7Fe_3-type unit cell.

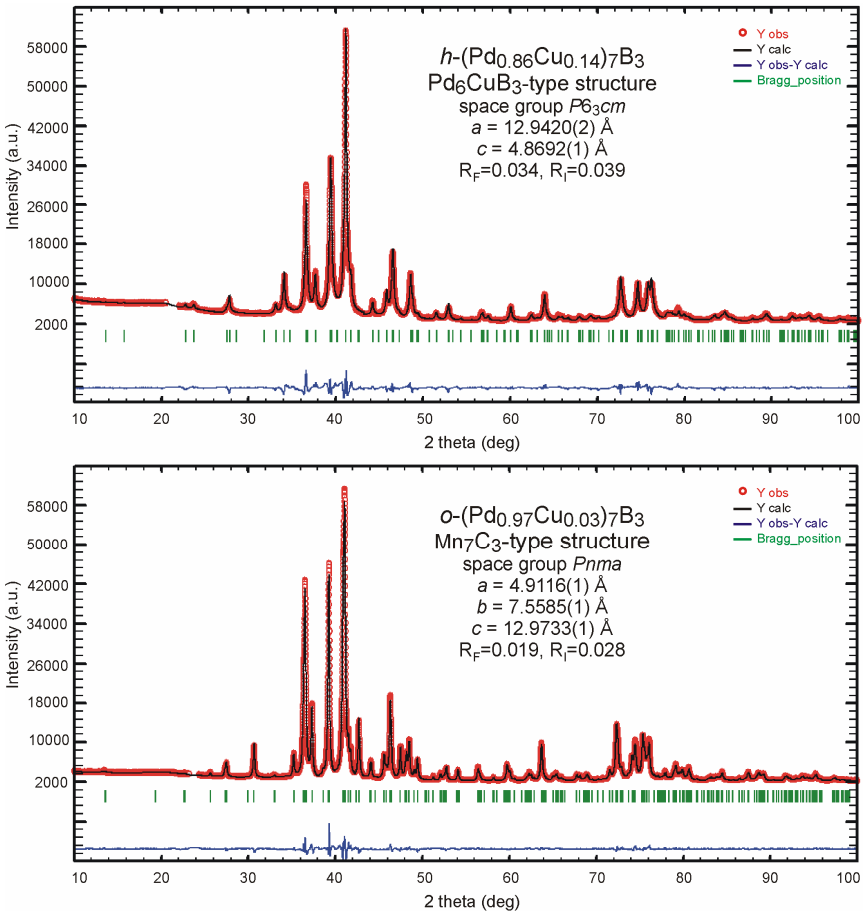

Figure 2 Supporting Information. Rietveld refinement of X-ray powder diffraction intensity data of $Pd_{60}Cu_{10}B_{30}$ (Pd_6CuB_3-type structure) and $Pd_{68}Cu_2B_{30}$ (Mn_7C_3-type structure) annealed at 650 °C.

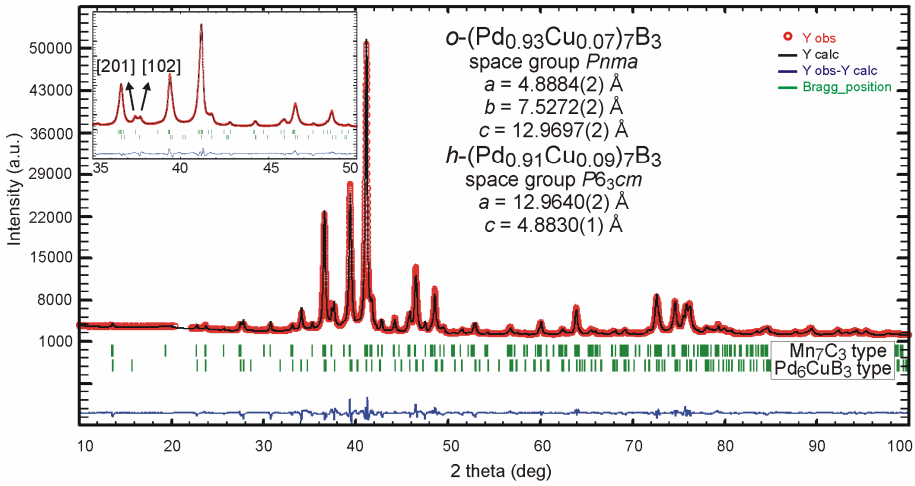

Figure 3 Supporting Information. Rietveld X-ray powder diffraction refinement of $Pd_{64}Cu_6B_{30}$ alloy annealed at 650 °C revealing the existence of orthorthombic Mn_7C_3-type and hexagonal Pd_6CuB_3-type phases.

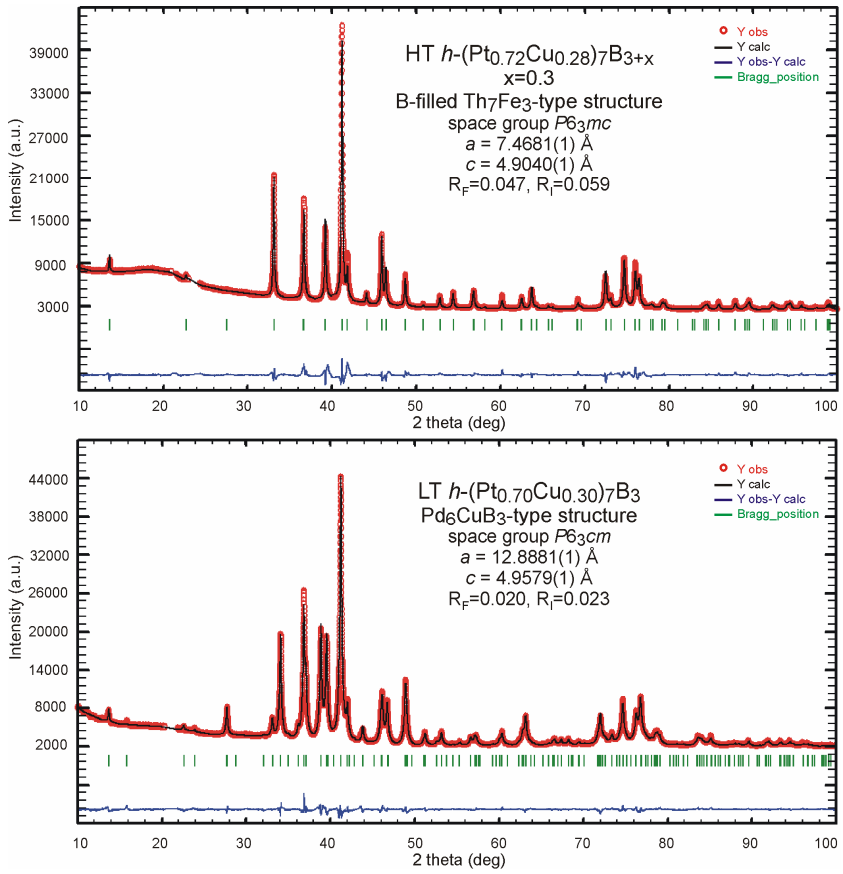

Figure 4 Supporting Information. Rietveld refinement of X-ray powder diffraction intensity data of as cast $Pt_{50}Cu_{18}B_{32}$ sample (B-filled Th_7Fe_3-type, x value fixed in correspondence with results of SC XRD) and $Pt_{49}Cu_{21}B_{30}$ sample annealed at 600 °C (Pd_6CuB_3-type)

Cu/Pt mixtures in the structures of both HT- and LT-phases reside predominantly at all tetrahedral sites while octahedral sites exhibit only minor replacement of platinum by copper (Table 3 Supporting Information). A similar tendency in site occupancies has been observed for the $Rh_{7-x}M_xB_3$ (M = Cr, Mn, Fe, Co, Ni)[17] phases of Th_7Fe_3-type where M was found to mix with rhodium at only one tetrahedral 6*c* site at x≤1 but after increasing the amount of M, particularly of iron in $FeRh_6B_3$ to produce, for example, the $Fe_{1.3}Rh_{5.7}B_3$, the additional iron atoms substitute rhodium in the tetrahedral 2*b* site, thereby leaving only one octahedral 6*c* site unaffected. For the copper-rich end of $(Pt_{0.72-y}Cu_{0.28+y})_7B_{3+x}$ range (y≅0.07-0.16), the similarities in the X-ray powder patterns with the Ca_7Au_3-type[12] structure have been elucidated, e.g. a=4.9248(4) Å, b=14.563(1) Å, c=12.920(1) Å in space group *Pbca* for the $Pt_{44}Cu_{26}B_{30}$ alloy annealed at 600 °C, however the poor values of reliability factors of Rietveld refinement (R_F=0.10, R_I=0.16) did not provide sufficient proofs for the correct choice of the structure model.

Our verification of the boundary Pd-B binary system in the relevant concentration and temperature ranges showed good agreement with literature data revealing the existence of three phases, namely Pd_2B, Pd_5B_2 and Pd_3B as well as the absence of Th_7Fe_3-type structure[36,37]. Traces of an unknown phase noticed on prolonged annealing at 600 °C (480 hours), has obviously indicated the formation of a low temperature unknown "Pd_5B" structure. The recent studies on the Pt-B binary boundary[38] yielded no formation of a Th_7Fe_3-type phase as well. Since no homologues binary palladium and platinum borides have been found to exist, the formation of the ternary phases is apparently a consequence of an electronic stabilizing effect of alloying element atoms.

Table 3 Supporting Information. Results of X-ray powder Rietveld refinement of LT *h*-$(Pt_{0.70}Cu_{0.30})_7B_3$

structure type	Pd_6CuB_3
composition (Rietved refinement)	$Pt_{4.9}Cu_{2.1}B_3$
composition (EPMA)	$Pt_{4.85}Cu_{2.15}B_3$
space group	$P6_3cm$, no. 185
lattice parameters [Å]	a=12.8881(1), c=4.9579(1)
volume [Å^3]	713.19(1)
ρ_{calc} [g cm^{-3}], Z	15.60, 6
range for data collection	$8°<\theta<100°$
reflections in refinement	190
number of variables	61
reliability factors[b]	R_F=0.020, R_I=0.023, R_{exp}=0.016, χ^2=3.08
M1 in 12*d*[a];	x=0.2061(1); y=0.5402(1); z=0.3811(2);
occ.; B_{iso}[c]	0.93(1)Pt1+0.07(1)Cu1;0.68(4)
M2 in 12*d*;	x=0.2071(1); y=0.3333(2); z=0.1762(3);
occ.; B_{iso}	0.46(1) Pt2+0.54(1)Cu2; 0.72(3)
M3 in 6*c*;	x=0.3376(2); z=0.2150(4);
occ.; B_{iso}	0.68(1)Pt3+32(1)Cu3; 0.60(4)
M4 in 6*c*;	x=0.1239(1); z=0.0000[d];
occ.; B_{iso}	0.85(1)Pt4+0.15(1)Cu4; 0.46(2)
M5 in 6*c*;	x=0.5580(2); z=0.2608(4);
occ.; B_{iso}	0.55(1)Pt5+0.45(1)Cu5; 0.48(3)
B1 in 12*d*;	x=0.324(1); y=0.474(1); z=0.470(3);
occ.; B_{iso}	1.00 B1; 0.8[d]
B2 in 6*c*;	x=0.193(2); z=0.399(4);
occ.; B_{iso}	1.00 B2; 0.8[d]

[a] atom coordinates are standardized using the program Structure Tidy[22], [b] $R_F=\Sigma|F_o-F_c|/\Sigma F_o$, $R_I=\Sigma|I_o-I_c|/\Sigma I_o$, $R_{exp}=[(N-P+C)/\Sigma w_i y^2_{oi})]^{1/2}$, $\chi^2=(R_{wP}/R_e)^2$, [c] isotropic atomic displacement parameters [Å^2], [d] fixed parameters

Electrical Resistivity. Concluding from resistivity data, the compounds $Pt_{4.9}Cu_{2.1}B_3$ (Pd_6CuB_3-type), $Pt_{5.04}Cu_{1.96}B_{3.3}$ (B-filled Th_7Fe_3-type), $Pd_{6.504}Cu_{0.496}B_3$ (Mn_7C_3-type) and $Pd_{6.047}Cu_{0.953}B_3$ (Pd_6CuB_3-type) are metallic in the temperature range from 1 to 300 K (Figure 8). Below 1 K, however $Pt_{4.9}Cu_{2.1}B_3$ and $Pt_{5.04}Cu_{1.96}B_{3.3}$ exhibit a superconducting transition at 0.67 and 0.66 K, respectively. $Pd_{6.504}Cu_{0.496}B_3$ and $Pd_{6.047}Cu_{0.953}B_3$, on the other hand, show superconductivity at temperatures close to the experimental limit.

The normal state resistivity curves for $Pd_{6.504}Cu_{0.496}B_3$ and $Pd_{6.047}Cu_{0.953}B_3$ were analyzed in scope of the Bloch-Grüneisen-Mott relation,

$$\rho_{B-G-M} = \rho_0 + C\frac{T^5}{\theta_D{}^6}\int_0^{\theta_D/T}\frac{x^5}{(e^x-1)(1-e^{-x})}dx - A_M T^3 \qquad (1)$$

where ρ_0 is a residual resistivity at 0 K, θ_D is a Debye temperature and a Mott-Jones term ($-A_M T^3$)[39] is added to the conventional Bloch –Grüneisen relation to account for the corrections due to scattering of conduction electrons on a narrow *d* band in the vicinity of the Fermi energy. Debye temperatures θ_D, residual resistivity values ρ_0 and Mott coefficients A_M obtained as the results of the fit of Eqn.1 to the appropriate experimental data are presented in Table 3, together with the residual resistivity ratios (RRR= ρ_{300}/ρ_N, where ρ_N is the value of the resistivity just above the superconducting transition) for the corresponding compounds.

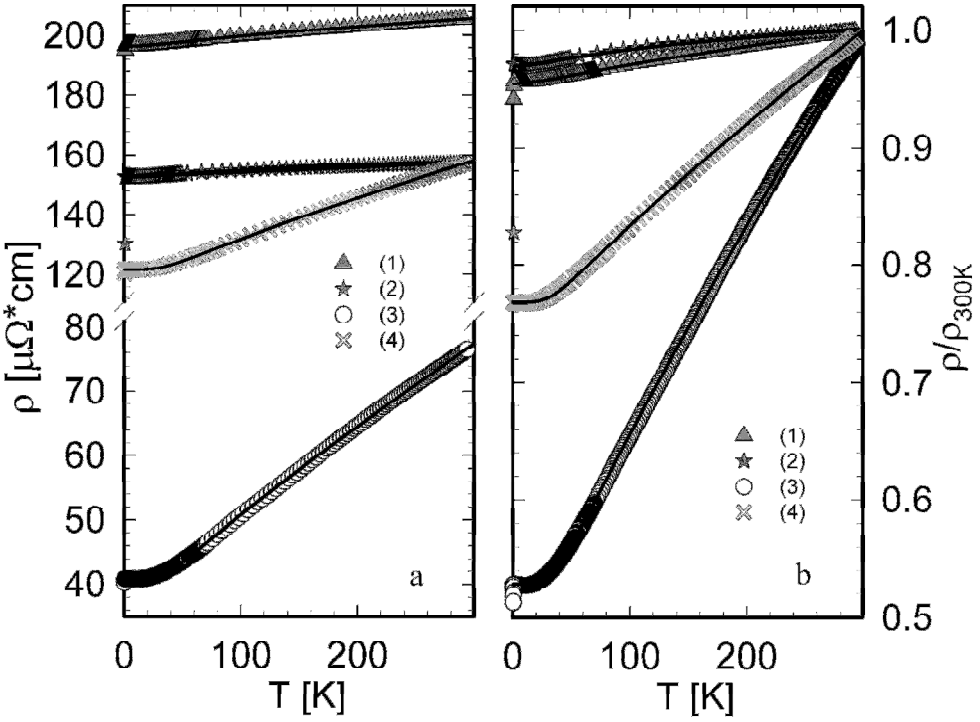

Figure 8. The electrical resistivity (a) and ρ/ρ_{300K} (b) of $Pt_{4.9}Cu_{2.1}B_3$, (Pd_6CuB_3-type) (1), $Pt_{5.04}Cu_{1.96}B_{3.3}$ (B-filled Th_7Fe_3-type) (2), $Pd_{6.504}Cu_{0.496}B_3$ (Mn_7C_3-type) (3) and $Pd_{6.047}Cu_{0.953}B_3$ (Pd_6CuB_3-type) (4). Solid lines correspond to models described in text.

Electrical resistivity of both $Pt_{4.9}Cu_{2.1}B_3$ and $Pt_{5.04}Cu_{1.96}B_{3.3}$, complimentary to the low RRR, demonstrates stronger curvature in the temperature region from 30 to 100 K and a tendency to saturate at higher temperatures. This feature no longer allows a description in terms of Eqn.1. Instead a good agreement was found between the experimental data of both compounds for temperatures from 10 to 300 K and a phenomenological model proposed by Woodard and Cody[40] to account for the resistivity of A15 superconductor Nb_3Sn,

$$\rho = \rho_0 + AT + Be^{(-C/T)}$$

where ρ_0 is the resistivity at low temperatures, A characterizes the growth of the resistivity at high temperatures and the exponential term is included to describe the unexpected rapid temperature dependence of the scattering probability in the low temperature region. The parameters obtained as a result of the least-square fits are listed in Table 3.

Table 3. Residual resistivity ratio and list square fit parameters $Pt_{4.9}Cu_{2.1}B_3$, (Pd_6CuB_3-type), $Pt_{5.04}Cu_{1.96}B_{3.3}$ (B-filled Th_7Fe_3-type), $Pd_{6.504}Cu_{0.496}B_3$ (Mn_7C_3-type) and $Pd_{6.047}Cu_{0.953}B_3$ (Pd_6CuB_3-type)

	ρ_0, [$\mu\Omega$cm]	θ_D [K]	A_M [10^{-8} $\mu\Omega$cm/K^3]	A [$\mu\Omega$cm/K]	C [K]	*RRR*
$Pt_{4.9}Cu_{2.1}B_3$	196.2	—	—	0.025	109.8	1.04
$Pt_{5.04}Cu_{1.96}B_{3.3}$	152.6	—	—	0.0081	74.0293	1.03
$Pd_{6.504}Cu_{0.496}B_3$	40.9	216.6	1.6	—	—	1.89
$Pd_{6.047}Cu_{0.953}B_3$	121.6	203.9	3.7	—	—	1.30

To get a deeper insight into the behavior of $Pt_{4.9}Cu_{2.1}B_3$, and $Pt_{5.04}Cu_{1.96}B_{3.3}$ their upper critical fields were studied and analyzed. The curves of the electrical resistivity obtained at various externally applied magnetic fields are displayed in Figure 9. An application of magnetic fields reduces the superconducting transition temperature, which becomes zero at the upper critical magnetic field $\mu_0 H_{C2}(0)$. Whereas for $Pt_{4.9}Cu_{2.1}B_3$, the superconducting transition can still be observed at magnetic fields as high as 0.27 T, the 0.25 T resistivity curve of $Pt_{5.04}Cu_{1.96}B_{3.3}$ reveals only the weakly noticeable onset of the transition, while the transition itself happens below the lowest temperature reachable in our setup. For both compounds the superconducting transition is completely suppressed at magnetic fields higher then 0.5 T.

The temperature dependent upper critical magnetic field was analyzed using a Werthamer, Helfand, and Hohenberg (WHH) model[41] that considers both orbit-depairing and Pauli mechanisms for the destruction of the Cooper pairs. Corresponding to this model, the temperature dependence of the upper critical field is determined by the transition temperature T_C, the slope of the upper critical field at the transition temperature $\left.\frac{d[\mu_0 H_{C2}(T)]}{dT}\right|_{Tc}$, the Maki parameter α_M and spin-orbit coupling λ_{SO}, where $\left.\frac{d[\mu_0 H_{C2}(T)]}{dT}\right|_{Tc}$ can be directly measured from a linear approximation of the experimental data near the transition temperature and the Maki parameter can be calculated as $\alpha_M = \frac{3e^2 \mathrm{h} \gamma \rho_0}{2m\pi^2 k_B^2}$. In our case the lack of heat capacity data makes it impossible to directly calculate α_M, rather it was obtained as

$\alpha_M = 5.3\times10^{-5}\left.\frac{-d[\mu_0 H_{C2}(T)]}{dT}\right|_{T_C}$ [42] (see Table 4). It is important to note that the influence of λ_{SO} on the temperature dependence of the upper critical field is negligible if α_M is small. The value of λ_{SO} in our study is about 10 for both compounds; the values of the upper critical fields at $\mu_0 H_{C2}(0)$ are 0.37 and 0.27 T for $Pt_{4.9}Cu_{2.1}B_3$ and $Pt_{5.04}Cu_{1.96}B_{3.3}$, respectively.

$Pd_{6.504}Cu_{0.496}B_3$ and $Pd_{6.047}Cu_{0.953}B_3$ in the low temperature limit hint to the onset of superconductivity by a small resistivity drop (Figure 9d).

Table 4. Parameters describing the behavior of the temperature dependent upper critical magnetic field for $Pt_{4.9}Cu_{2.1}B_3$ and $Pt_{5.04}Cu_{1.96}B_{3.3}$

	T_C [K]	$\left.\frac{d[\mu_0 H_{C2}(T)]}{dT}\right\|_{Tc}$ $[\mu_0(T/K)]$	α_M	λ_{SO}
$Pt_{4.9}Cu_{2.1}B_3$	0.67	-0.8	0.42	~10
$Pt_{5.04}Cu_{1.96}B_{3.3}$	0.66	-0.6	0.32	~10

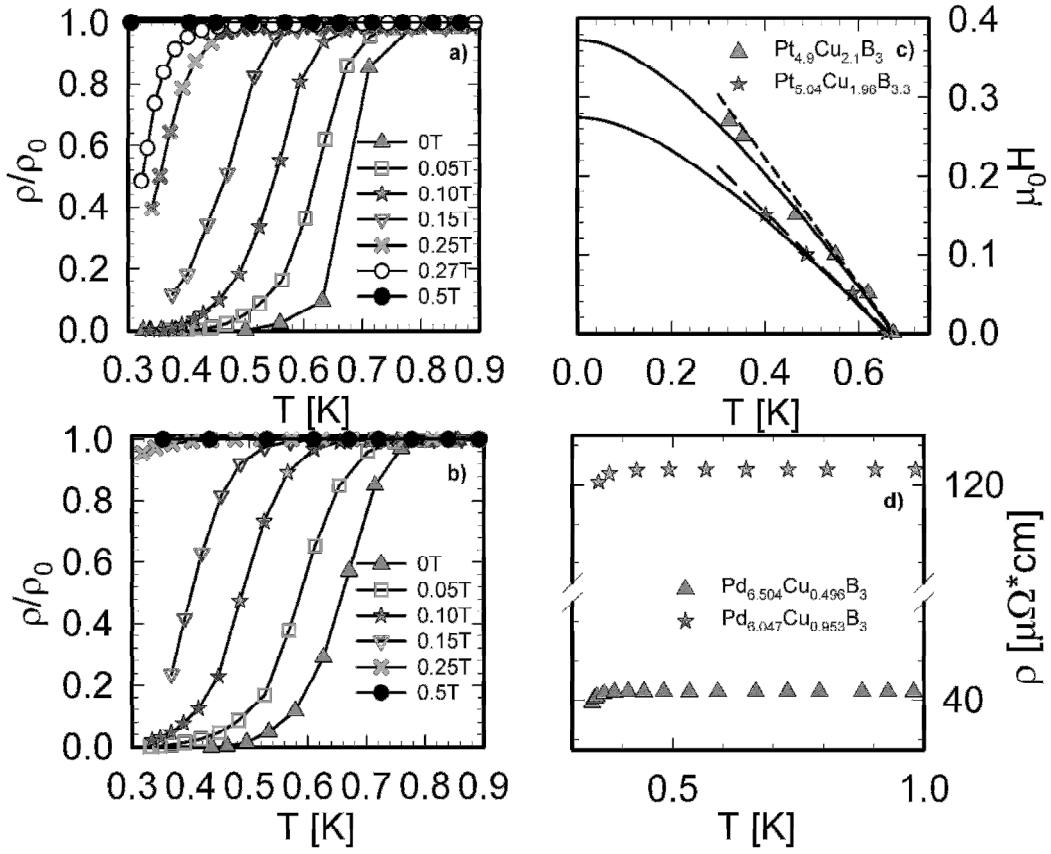

Figure 9. Evolution of the electrical resistivity under the influence of magnetic fields of $Pt_{4.9}Cu_{2.1}B_3$ (a), $Pt_{5.04}Cu_{1.96}B_{3.3}$ (b) and their temperature dependent upper critical fields $\mu_0 H_{C2}(T)$ (c). Electrical resistivity of $Pd_{6.504}Cu_{0.496}B_3$ and $Pd_{6.047}Cu_{0.953}B_3$ in the low temperature region. The drop in $\rho(T)$ is attributed to the onset of superconductivity (d).

Conclusions

The current study expanded the knowledge on the Th_7Fe_3-type derivative structures introducing a new member of the boride family which exhibits a hitherto unknown structure type, Pd_6CuB_3 (space group $P6_3cm$, a=1.29426(9) nm, c=0.48697(4) nm for *h*-$(Pd_{0.864}Cu_{0.136})_7B_3$). Besides, at slightly higher palladium content a first boride representative of the orthorhombic Mn_7C_3-type has been found to exist in the Pd-Cu-B system: *o*-$(Pd_{0.93}Cu_{0.07})_7B_3$, (space group *Pnma*, a=0.48971(2) nm, b=0.75353(3) nm, c=1.29743(6) nm). Furthermore, in the Pt-Cu-B system, single crystal data of HT *h*-$(Pt_{0.717}Cu_{0.283})_7B_{3+x}$ (space group $P6_3mc$, a=0.74424(12) nm, c=0.48549(8) nm) have proven a new B-filled structure variant of Th_7Fe_3-type which exhibited a partial B-occupancy of octahedral [Pt_6] voids whereas the low-temperature phase was observed to form the Pd_6CuB_3-type structure (space group $P6_3cm$, a=1.28996(1) nm, b=0.49635(1) nm for LT *h*-$(Pt_{0.70}Cu_{0.30})_7B_3$) from Rietveld refinement of X-ray powder data of alloys annealed at 600 °C. The core part of the all three structures is built of columns of face-connected metal octahedra and columns of condensed alternatively via common vertices and faces metal tetrahedra. Boron atoms fill the trigonal prismatic voids within the metal atom frameworks in the three structures as well as partially fill the octahedral voids in the structure of HT *h*-$(Pt_{0.717}Cu_{0.283})_7B_{3+x}$ (B-filled Th_7Fe_3-type). The unit cell of B-filled Th_7Fe_3-type structure contains one octahedral column and two tetrahedral columns running infinitely along the short axis; the relative positioning of the columns implies that three equi-latitudinal trigonal prismatic voids per octahedron and tetrahedron are occupied by boron leaving unoccupied the voids adjacent to every next tetrahedron in the column. In both Mn_7C_3- and Pd_6CuB_3-type structures, the boron atoms fill two voids adjacent to one tetrahedron and one void adjacent to the consecutive tetrahedron along the column. While in the Mn_7C_3-type structure, one of every two octahedral columns is rotated around the short axis by 60° with respect to the other, in Pd_6CuB_3, ⅔ of the octahedral columns are displaced giving rise to a new structure. The fourth member of the series of Th_7Fe_3-type related structures, the Ca_7Au_3 structure[12] (and isotypic *o*-Fe_7C_3 compound recently discovered[11]) exhibits the arrangement of four octahedral columns in the unit cell, two of which are rotated around the short axis by 60° with respect to the others. Thus the volumes of the HT *h*-$(Pt_{0.717}Cu_{0.283})_7B_{3+x}$, *o*-$(Pd_{0.93}Cu_{0.07})_7B_3$, *h*-$(Pd_{0.864}Cu_{0.136})_7B_3$ and insinuated from refinement of X-ray powder diffraction data the Ca_7Au_3-type derivative platinum copper boride relate as 1:2:3:4, respectively.

The increase of Pd content on progressing from the Cu-rich to Cu-poor members within the range of existence of Th_7Fe_3-type derivative structures ($Pd_{58.5}Cu_{11.5}B_{30}$-$Pd_{68.5}Cu_{1.5}B_{30}$ at 650 °C) is realized via continuous decrease of Cu occupancy at tetrahedral Cu2 and Cu5 sites (12*d*, 6*c* and 8*d,* 4*c* in Pd_6CuB_3- and Mn_7C_3-type structures, respectively) up to complete vanishing of Cu in 4*c* atom site of the orthorhombic unit cell of $(Pd_{0.979}Cu_{0.021})_7B_3$. In the Pt-Cu-B system, the Pt-rich end (HT *h*-$(Pt_{0.72-y}Cu_{0.28+y})_7B_{3+x}$, y≅0-0.07, x≅0-0.3) of the Th_7Fe_3-type derivative phase field in as cast conditions forms a small hexagonal lattice of B-filled Th_7Fe_3-type which on annealing at 600 °C decomposes to the low temperature form of Pd_6CuB_3-type. Cu/Pt mixtures in the structures of both HT- and LT-phases reside predominantly at all tetrahedral sites whereas the octahedral sites exhibit minor replacement of Pt by Cu. As inferred by Rietveld refinement of X-ray powder diffraction data and EDX analysis, the Ca_7Au_3-type derivative boride exists in the $(Pt_{0.72-y}Cu_{0.28+y})_7B_{3+x}$ (y≅0.07-0.16, x≅0-0.3) range both in as cast and annealed alloys.

Two new platinum containing boride systems $Pt_{4.9}Cu_{2.1}B_3$ (Pd_6CuB_3-type) and $Pt_{5.04}Cu_{1.96}B_{3.3}$ (B-filled Th_7Fe_3-type) exhibit a superconducting transition at 0.67 K and 0.66 K, respectively. Such a small difference of the transition temperatures can not be accidental and most likely is a result of the influence of the common structural features of the two compounds. Considering this, one may treat the increase in the value of the upper critical field as the result of an increased amount of defects serving as pinning centers for the flux line lattice. Such a conclusion is supported by a 25 percent higher residual resistivity value found for $Pt_{4.9}Cu_{2.1}B_3$. However, Orlando et al. (1979)[43] argue that the same mechanism should slightly decrease the superconducting transition temperature.

Experimental Section

Synthesis, phase analysis and X-ray powder diffraction studies. Alloys were prepared from ingots of thoroughly re-melted pieces of palladium or platinum foil or sponge (Ögussa, Austria, 99.99 mass%), Cu shot (2-6mm, 99.999 mass%, ChemPur, Germany) and crystalline boron (ChemPur, Germany, 99.4 mass%) by repeated arc melting under argon. The arc-melted buttons were wrapped in tantalum foil and vacuum-sealed in a quartz tube for annealing at 600 °C (650 °C) for 240 hours. Lattice parameters and standard deviations were determined by least squares refinement of room temperature X-ray powder diffraction data obtained from a Guinier-Huber image plate employing monochromatic $CuK_{\alpha 1}$ radiation and Ge as internal standard (a_{Ge}=5.65791 Å). Qualitative analysis has been performed from the results of Rietveld refinements of X-ray powder diffraction data (program FULLPROF[44]).

For precise quantitative analysis of the Pd (Pt)/Cu ratio, the samples were polished using standard procedure and were examined by scanning electron microscopy (SEM/EDX) using a Philips XL30 ESEM with EDAX XL-30 EDX-detector.

Electrical resistivity. Electrical resistivity was measured on 1×1×4 mm size bar specimen applying a standard 4-point technique with an a. c. bridge (Lakeshore 370 AC Resistance Bridge) in a temperature region from 0.3 to 300 K and in magnetic fields up to 1T.

Single crystal X-ray diffraction studies. Single crystals suitable for X-ray diffraction studies were isolated from fragmented alloys. The crystals were measured on a four-circle Bruker APEX II diffractometer equipped with a CCD detector (κ-geometry, Mo Kα radiation); orientation matrices and unit cell parameters were derived with the APEX II software.[45] Multi-scan absorption correction was applied using the program SADABS; frame data were reduced to intensity values applying the SAINT-Plus package.[46] The structures were solved by direct methods and refined with the SHELXS-97 and SHELXL-97 programs,[47,48] respectively. Further details concerning the experiments are summarized in Table 1.

Structure determination for HT *h*-($Pt_{0.717}Cu_{0.283}$)$_7B_{3+x}$, x=0.28 (≡$Pt_{5.02}Cu_{1.98}B_{3.28}$). X-ray single crystal diffraction data indexing for the crystal selected from the as-cast alloy $Pd_{45}Cu_{20}B_{35}$ led to a hexagonal unit cell with lattice constants a=7.4424(12) Å and c=4.8549(8) Å. The observed extinctions were compatible with the space groups $P6_3/mmc$, $P\text{-}62c$ and $P6_3mc$ (WinGX program package[49]) of which the noncentrosymmetric $P6_3mc$ was confirmed to be correct by subsequent successful structure solution and refinement against F^2. Structure solution applying direct methods resulted in three metal atom positions, one of which (6*c*) was assigned to Pt while the remaining two (6*c* and 2*b)* showed considerably smaller electron densities; refinement of occupancy parameters, assuming mixed population for these atom sites, resulted in M2=44.6% Pt2+55.4% Cu2 and M3=68.1% Pt3+31.9% Cu3, respectively. Two boron atom sites - 6*c* and 2*a* - were located from the analysis of electron density peaks in difference Fourier maps according to reasonable interatomic distances between detected and proposed atoms, among them the 2*a* site was found to be occupied for about 30%. Refinement converged to a reliability factor as low as R_{F2}=0.0285 applying anisotropic displacement parameters for the metal atoms and constrained isotropic displacement parameters for borons (Tables 1, 2, Table 1 Supporting Information).

Structure determination for *h*-($Pd_{0.864}Cu_{0.136}$)$_7B_3$ (≡$Pd_{6.047}Cu_{0.953}B_3$). X-ray diffraction data for the crystal, which was selected from the alloy $Pd_{58}Cu_{10}B_{32}$ annealed at 600 °C, were indexed with a primitive hexagonal unit cell with lattice parameters a=12.9426(9) Å and c=4.8697(4) Å. Systematic absences in the diffraction data were consistent with three space

groups, $P6_3/mcm$, $P\text{-}6c2$ and $P6_3cm$ (WinGX program package[49]), of which non-centrosymmetric $P6_3cm$ proved to be correct during structure solution and refinement. Five palladium atom positions have been assigned and refined in a straightforward manner; two palladium sites exhibited relatively large displacement parameters suggesting that they are disordered with copper atoms (M2=0.627 Pd2+0.373 Cu2 in 12*d* and M5=0.793 Pd5+0.207 Cu5 in 6*c*). Two boron sites were easily located in the difference Fourier map. Refinement of occupancy and displacement parameters proceeded successfully to a small residual value (R_{F2}=0.0263, max/min residual electron density 1.59/-1.51 el/Å^3) (Tables 1-2, Table 1 Supporting Information).

Structure determination for *o*-$(Pd_{0.93}Cu_{0.07})_7B_3$ (≡$Pd_{6.504}Cu_{0.496}B_3$). The unit cell parameters of the single crystal obtained from the $Pd_{65}Cu_5B_{30}$ sample annealed at 600 °C (orthorhombic *P*, a=4.8971 Å, b=7.5353 Å, c=12.9743 Å) and X-ray powder diffraction spectra recorded from both the annealed and as-cast alloys suggested isotypism with the Mn_7B_3–type structure.[10] Systematic extinctions in the single crystal X-ray data were consistent with two possible space group types: centrosymmetric *Pnma* (no. 62) and non-standard setting of non-centrosymmetric $Pn2_1a$ (no. 33). The structure was solved in the centrosymmetric space group and direct methods provided 5 atom positions of palladium. The refinement of the structure with all sites fully occupied yielded rather large anisotropic displacement parameters for two Pd sites, Pd2 and Pd5; refinement of occupancy parameters - assuming mixed population for these atom sites - resulted in 78.6% Pd2+21.4% Cu2 and 93.2% Pd5+6.8% Cu5, respectively. The atom positions of boron atoms were derived from difference Fourier synthesis. Refinement of the structure with anisotropic displacement parameters for metal atom sites converged to R=0.0247 with residual electron densities smaller than 1.237 el/Å^3 (Tables 1, 2, Table 1 Supporting Information).

Further details of the single crystal structure determination may be obtained from the Fachinformationszentrum Karlsruhe, 76344 Eggenstein Leopoldshafen, Germany (Fax: (+49)7247-808-666; e-mail: crysdata@fiz-karlsruhe.de), quoting the depository numbers CSD-.... (HT *h*-$(Pt_{0.717}Cu_{0.283})_7B_{3+y}$ (y=0.28), CSD-.... (*h*-$(Pd_{0.864}Cu_{0.136})_7B_3$) and CSD-.... (*o*-$(Pd_{0.93}Cu_{0.07})_7B_3$).

Acknowledgements

The research work of O.S. was supported by Austrian FWF project V279-N19. L.S. is grateful to ÖAD for a research fellowship. Authors are very thankful to Dr. Klaudia Hradil (XRC TU Wien) for collaboration.

References

[1] J. V. Florio, N. C. Baenziger, R. E. Rundle, *Acta Cryst.* 1956, *9*, 367.

[2] H. C. Eckstrom, W. A. Adcock, *J. Am. Chem. Soc*. 1950, *72 (2)*, 1042–1043.

[3] A. Wiengmoon, T. Chairuangsri, J. T. H. Pearce, *Key Eng. Mat*. 2015, *658*, 76-80.

[4] J. T. H. Pearce, *Foundryman* 2002, *95*, 156-166.

[5] C. P. Tabrett, I. R. Sare, M. R. Ghomashchi, *Int. Mater. Rev*. 1996, *41*, 59–82.

[6] G. Laird, R. Gundlach, K. Rohrig, *Abrasion-resistant Cast Iron Handbook*, Des Plaines, III: Am. Foundry Soc., IL, USA, 2000.

[7] J. P. Morniroli, M. K. Khachfi, A. Courtois, J. Mahy, D. van Dyck, J. van Landuyt, S. Amelinckx, *Philos. Mag. A*, 1987, *56(1)* 93-113.

[8] M. Kowalski, *J. Appl. Cryst*. 1985, *18*, 430-435.

[9] B. Aronsson, *Acta Chem. Scand*. 1959, *13*, 109-114.

[10] R. Fruchart, A. Rouault, *Ann. Chim. (Paris)*, 1969, *4*, 143-145.

[11] C. Prescher, L. Dubrovinsky, E. Bykova, I. Kupenko, K. Glazyrin, A. Kantor, C. McCammon, M. Mookherjee, N. Nakajima, N. Miyajima, R. Sinmyo, V. Cerantola, N. Dubrovinskaia, V. Prakapenka, R. Ruffer, A. Chumakov, M. Hanfland, *Nat. Geosci*. 2015, 8220.

[12] M. L. Fornasini, F. J. Merlo, *Solid State Chem*. 1985, *59*, 65–70.

[13] B. Aronsson, E. Stenberg, J. Aselius, *Acta Chem. Scand*. 1960, *14*, 733-741.

[14] W. Trzebiatowski, J. Rudzinski, *J. Less-Common Met*. 1964, *6*, 244-245.

[15] K. Hofmann, N. Kalyon, Ch. Kapfenberger, L. Lamontagne, S. Zarrini, R. Berger, R. Seshadri, B. Albert, *Inorg. Chem*. 2015, *54*, 10873−10877.

[16] Yu. B. Kuzma, N. V. Chaban, *Binary and Ternary Systems Containing Boron*, Metallurgiya, Moskva, 1990.

[17] P. R. N. Misse, M. Gilleßen, B. P. T. Fokwa, *Inorg. Chem*. 2011, *50*, 10303-10309.

[18] E. Bauer-Grosse, J. P. Morniroli, M. Khachfi, M. Gantois, T. Lundström, A. Courtois, *J. Less Comm. Met*. 1986, *117 (1–2)*, 231–236.

[19] O. Sologub, P. Rogl, G. Giester, *Intermetallics*, 2010, *18(4)*, 694-701.

[20] L. P. Salamakha, O. Sologub, B. Stöger, H. Michor, E. Bauer, P. F. Rogl, *J. Solid State Chem*. 2015, *229*, 303-309.

[21] O. Sologub, L. P. Salamakha, G. Eguchi, B. Stöger, P.F. Rogl, E. Bauer, Boron induced structure modifications in Pd-Cu-B system: new Ti_2Ni-type derivative borides Pd_3Cu_3B and $Pd_5Cu_5B_2$, *Dalton Trans*. 2016, DOI: 10.1039/C5DT05058H.

[22] E. Parthé, L. Gelato, B. Chabot, M. Penzo, K. Censual, R. Gladyshevskii, *TYPIX – Standardized Data and Crystal Chemical Characterization of Inorganic Structure Types*, Springer, Berlin, 1994.

[23] P. I. Krypyakevych, *Structure Types of Intermetallic Compounds*, Nauka, Moskva, 1977

[24] A. Westgren, *Jernkontorets Ann*. (1935) 118, 231-240.

[25] F. H. Herbstein, J. A. Snyman, *Inorg. Chem*. 1964, *3(6)*, 894-896.

[26] F. X. Kayser, *Mat. Res. Bull*. 1996, *31(6)*, 635-638.

[27] M. Durand-Charre, *Microstructure of Steels and Cast Irons*, Springer-Verlag, Berlin-Heidelberg-New York, 2004.

[28] M. A. Rouault, P. Herpin, M. R. Fruchart, *Ann. Chim*. 1970, *5*, 461-470.

[29] V. S. Telegus, Y. B. Kuz'ma, *Visn. L'viv. Derzh. Univ. (Ser. Khim.)*, 1971, *12*, 28.

[30] W. Koch, H. Kolbe-Rohde, *Z. Anorg. Allg. Chem*. 1963, *319*, 312-319.

[31] P. Stecher, F. Benesovsky, H. Nowotny, *Planseeber. Pulvermetall*. 1964, *12*, 89-95.

[32] B. Kaplan, A. Markström, S. Norgren, M. Selleby, *Met. Mat. Trans. A*, 2014, *45A*, 4820-4828.

[33] M. M. Filipović, *Hem. Ind*. 2014, *68 (4)*, 413–427.

[34] B. Kaplan, A. Blomqvist, C. Århammar, M. Selleby, S. Norgren, *Structural determination of* $(Cr,Co)_7C_3$ in: 18th Plansee Seminar, 2013, Int. Conf. Refractory Metals and Hard Materials, Reutte, Austria, 3-7 June, 2013, HM 104/1.

[35] T. Sterneland, J. Xie, N. Chen, S. Seetharaman, *Scr. Mater*. 2006, *54*, 1491–1495.

[36] H. Ipser, P. Rogl, *J. Less Com. Met*. 1981, *82(1-2)*, 363.

[37] O. Sologub, P. Rogl, L. Salamakha, E. Bauer, G. Hilscher, H. Michor, G. Giester, *J. Solid State Chem*. 2010, *181(5)*, 1013-1037.

[38] O. Sologub, L.P. Salamakha, P. Rogl, B. Stöger, E. Bauer, J. Bernardi, G. Giester, M. Waas, R. Svagera, *Inorg. Chem*. 2015, *54 (22)*, 10958–10965.

[39] O. Gunnarsson, M. Calandra, J. E. Han, *Rev. Mod. Phys*. 2003, *75*, 1085.

[40] D. W. Woodard, G. D. Cone, *Phys. Rev*. 1964, *136*, A166.

[41] N. R. Werthamer, E. Helfand, P. C. Hohenberg, *Phys. Rev*. 1966, *147*, 295.

[42] K. Maki, *Phys. Rev*. 1966, 148, 362.

[43] T. P. Orlando, E. J. McNiff, S. Foner, M. R. Beasley, *Phys. Rev. B*, 1979, *19*, 4545.

[44] J. Rodriguez-Carvajal, *Physica B* 1993, *192*, 55-69.

[45] *Bruker Advanced X-ray solutions*. APEX2 User Manual. Version 1.22. 2004, Bruker AXS Inc.

[46] Bruker. APEXII, SAINT and SADABS. 2008, Bruker Analytical X-ray Instruments, Inc., Madison, Wisconsin, USA.

[47] G. M. Sheldrick, *SHELXS-97, Program for the Solution of Crystal Structures*. University of Göttingen, Germany, 1997.

[48] G. M. Sheldrick, *SHELXL-97, Program for Crystal Structure Refinement*. University of Göttingen, Germany, 1997.

[49] L. J. J. Farrugia, *Appl. Cryst*. 1999, *32*, 837-838.